Metaheuristic-Based Control for Three-Phase Grid-Connected Solar Photovoltaic Systems

Afef Badis, National Engineering School of Monastir, Tunisia*

iD https://orcid.org/0000-0003-0473-2340

Mohamed Habib Boujmil, Higher Institute of the Technological Studies of Nabeul, Tunisia

Mohamed Nejib Mansouri, National Engineering School of Monastir, Tunisia

ABSTRACT

In this paper, a novel cascade control technique is proposed in order to identify the parameters of cascade controllers in a grid-connected photovoltaic (PV) system. Here, tuning of the inner and outer loop controllers is done simultaneously by means of an optimized genetic algorithm-based fractional order PID (GA-FOPID) control. Simulations are conducted using Matlab/Simulink software under different operating conditions, namely under fast-changing weather conditions, sudden parametric variations, and voltage dip, for the purpose of verifying the effectiveness of the proposed control strategy. By comparing the results with recently published optimization techniques such as particle swarm optimization (PSO) and ant colony optimization (ACO), the superiority and effectiveness of the proposed GA-FOPID control have been proven.

KEYWORDS

Ant Colony Optimization, Cascade Control, Energetic Macroscopic Representation, FOPID Controller, Genetic Algorithm, Grid-Connected Photovoltaic System, Particle Swarm Optimization

INTRODUCTION

The increasing global energy demand has led the world to exploit Solar Energy as an alternate energy source thanks to its availability, inexhaustible nature and cleanness. (Green, 2002; Xu, Moulema, Ge, Song, & Yu, 2016; Taylor, Koutroulis, &laabjerg, 2015).

To date, the grid-connected Photovoltaic (PV) systems are tremendously exploited in online applications. Generally, the compatibility with the grid utility is a challenging issue that numerous papers in the literature are trying to solve in order to enhance the efficiency of the grid-connected PV Generator (PVG) (Raducu, 2008; Badis, Boujmil, &Mansouri, 2019).

*Corresponding Author

The boosting and the inverting stages usually take place in the power conversion system. However, this system is known to suffer from the irregular behavior of the PV system. The unpredictable internal and external changes make the operating point vary due to the control unit and the parametric errors. In connection with these problems, the use of robust control laws is crucial for ensuring the stabilization and the good tracking. Interestingly, many researchers are working on the conversion chain of grid-connected PV systems (Alajmi, Ahmed, Finney, & Williams, 2011; Bo, Wuhua, Yi, & Xiangning, 2010; Kottas, Boutalis, & Karlis, 2006; Menniti, Pinnarelli, & Brusco, 2011).

Hence, the proposed grid-connected PV system has to guarantee the following threefold evaluations:

- Making the PV array operate at its Maximum Power Point (MPP) at all times.
- Tight control of the DC link voltage.
- Inject a harmonic free output power to the grid by using the DC/AC inverter.

In order to achieve those goals, there has been a considerable progress made in optimization techniques. Typically, a current controller with fast dynamic response and high performance is required to satisfy the standard specifications. Accordingly, the fundamental goals are to minimize the steady-state tracking error and to ensure that the system is stable and robust under varying system parameters, voltage dips, and uncertainties.

Several control approaches have been developed for grid-connected PV systems. Even though these control strategies can achieve the same targets, they differ quite considerably in performance. The Proportiaonal Integral Derivative (PID) controller has been significantly explored in many applications over the past decades since it performs well in linear systems as compared to many new advanced control strategies, namely model predictive control (Hu, Zhu, & Dorrell, 2015), fuzzy PI control (Thumu, & Harinadha Reddy, 2019; Ganesan, Vasant, Sanghvi, Thomas, & Litvinchev, 2020), neural control (Boumaaraf, Talha, & Bouhal, 2015), etc (Singh, & Padhy, 2017). However, these techniques vary in terms of complexity, speed and precision under special conditions such as varying parameters, the PID controller becomes unreliable.

To overcome aforementioned weaknesses, several researches have employed metaheuristic approaches such as Particle Swarm Optimization (PSO), Ant Colony Optimization (ACO), and Genetic Algorithm (GA) for the purpose of tuning the controller parameters. PSO was first developed by Kennedy, & Eberhart (1995), which has shown effectiveness in dealing with the nonlinear systems in several fields (Koad, Zobaa, & El-Shahat, 2017); Tayal, & Ravi, 2016). Owing to its simple structure and easy implementation, PSO can generate potential solutions with fast computation capability in designing and tuning a PID controller (Solihin, Tack, & Kean, 2011).

As the PID controller has been extensively applied in grid-connected PV systems, this controller will be assessed in this research to be compared with Fractional Order PID (FOPID). Fractional order controller, employing fractional order operators in its structure, provides better robustness and a higher degree of freedom when compared to integer-order controllers. By setting the appropriate fractional-I and fractional-D actions, the FOPID was firstly disclosed by Petráš, Dorčák, & Koštial (1998). Since then, FOPID controllers has concerned more researchers to reach the best performances of numerous systems (Chen, Bhaskaran, & Xue, 2008; Das, Pan, Das, & Gupta, 2012; Jeba, & Immanuel Selvakumar, 2018).

Cascade control is a commonly used complex control structures for improving the performance of the conventional single-loop. Although sophisticated cascade control schemes have been suggested (Kaya, Tan,& Atherton, 2007), the basic configuration always includes two loops which requires the tuning of two cascade controllers. Usually, parameters of the secondary controller is firstly optimized. Controller gains of the inner loop are then identified

in a strict sequence. This procedure is time consuming since it requires at least two tests to be executed (Liu, Gu, & Zhang, 2005). However, Malaterre, Dorchies, & Baume, (2014) has improved the tuning the sequential tuning so that only one trial is performed to adjust both controllers simultaneously.

To capitalize, a new FOPID controller is applied in order to control the grid-connected PV system which includes four cascade control loops. The control strategy performances are compared in terms of is insensitivity to parameter variations, perturbations, and irregularities with a traditional PID controller.

Conventionally, the parameters of the controllers in the primary and secondary loops are identified sequentially which leads to a difficult and time-consuming control.

The proposed controller is tuned by GA, a highly powerful tool for solving complex optimization topics. It searches simultaneously for the FOPID parameters of both the PVG and grid side cascade subsystems, that optimize the most the power transfer from the PVG to the grid and maintain the overall stability of the system.

The remainder of the present paper is organized as follows. Section 2 presents the mathematical modeling of the PV system and the fundamental transformations used in this study. This section is followed by the introduction of different control strategies. PID and FOPID controllers are tuned for the Grid-connected PV system using metaheuristic techniques in section 4. The performance of the proposed methods are evaluated and compared under various operating conditions. Advantages of FOPID tuned by GA are shown. Finally, Section 5 presents the conclusion of this research work followed by the future works.

MODELING OF THE GRID-CONNECTED PHOTOVOLTAIC SYSTEM

The following section presents the model and the detailed equations which describe the performance of each component in the PV conversion system. The chosen PV conversion system relies on extracting the maximum active power from the PVG through a boost converter operating with a suitable Maximum Power Point Tracking (MPPT) and delivering an almost harmonic free current into the three-phase grid via a voltage inverter.

The PV system modeling and the development of its appropriate control techniques require a basic representation of the entire system. The Energy Macroscopic Representation (EMR) is a graphical representation, which simultaneously depicts the basic representation of the global system as well as its chain of control (Lhomme, Delarue, Giraud, Lemaire-Semail, & Bouscayrol, 2012), for representation and modeling of different systems.

All components of the EMR based system are inter-connected so as to frame the EMR of the overall system, by following the action-feedback principle and by respecting the integrated causality by considering the outputs of the subsystem as the inputs of the next one, as shown in Figure 1. The used representation allows to understand the relations between all the system parameters and to conceive the system controllers. The maximum control structure (MCS) is deduced by inversion of the EMR and helps for modeling the control loops (Lhomme et al., 2012; Badis, Mansouri, & Boujmil, 2019).

The current electrical source (green oval) represents the PVG. An ideal photovoltaic cell is equivalent to a power source shunted by a diode as shown in Figure 2 (Tyukhov, Rezk, & Vasant, 2016).

G_{STC} Irradiance at STC = 1000 W/m^2
T_{STC} Temperature at STC=25°C

Figure 1. The EMR and its reverse MCS of the entire system
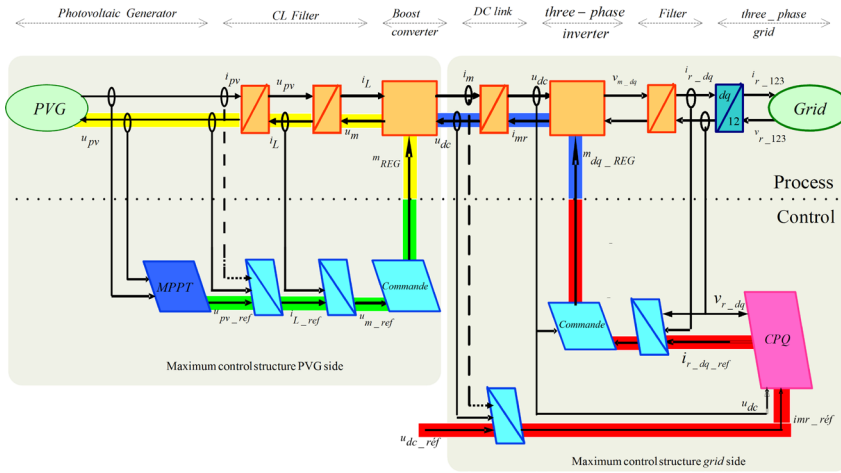
$$
\begin{cases}
I_{ph} = N_p \times i_{ph} : \text{photocurrent } N_p \text{ parallel cells.} \\
I_{pv} = N_p \times i_{pv} : \text{current supplied by } N_p \text{ parallel cells.} \\
I_s = N_p \times i_s : \text{reverse saturation current of } N_p \; diode \; in \; parallel \\
v_T = \dfrac{nK_B T}{q} \text{ is the thermodynamic potential} \\
N_p : \text{number of cells in parallel} \\
N_s : \text{number of cells in serie} \\
q : electron \; charge \, (1{,}6.10^{-19}\text{C}) \\
K_B : \text{Boltzman Constant} \, (1{,}38.10^{-23}\text{j/°K}). \\
T : \text{junction temperature °K.} \\
\text{n: ideality factor of the picture of the solar cell,} \\
\; \text{including between 1 and 5 in practice} \\
K_I \qquad \text{Coefficient temperature of short circuit current} \left(A \, / \, K\right) \\
U_{pv} \qquad \text{the PV voltage} \left(V\right) \\
v_{r1,2,3} \; \text{the grid voltages} \\
v_{m1,2,3} \, \text{the modulated voltages of inverter} \\
v_{rd,q} \quad \text{the grid voltages in dq reference frame} \\
v_{md,q} \quad \text{the modulated voltages of inverter in the dq reference frame} \\
u_m \text{the modulated voltage of the boost converter} \\
U_{dc} \text{DC link voltage} \\
i_{r1,2,3} \text{the grid currents} \\
i_{rd,q} \text{the grid currents in the dq reference frame} \\
i_m \text{the modulated current of boost converter} \\
i_{rm} \text{the modulated current of inverter}
\end{cases}
$$

Figure 2. Equivalent circuit model of a solar PV cell
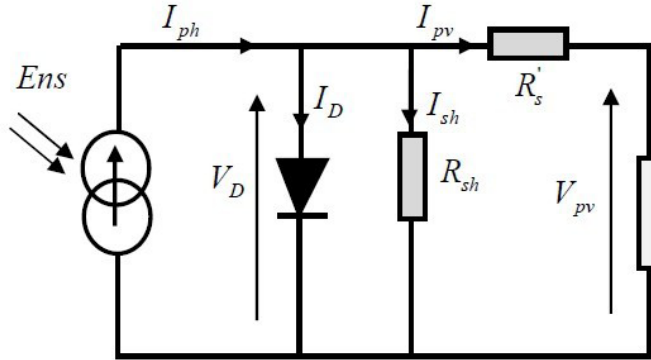
The photo current I_{ph} is defined by the following equation:

$$I_{ph} = I_D + I_{sh} + I_{pv} \tag{1}$$

The PV model containing N_s cells in series and N_p cells in parallel is mathematically modeled using Equation (2) shown below:

$$I_{pv} = Np\left(I_{ph} - I_0 \left(e^{\left(\dfrac{V_{pv} + R_{sg} I_{pv}}{N_s V_T} \right)} - 1 \right) \right) - \dfrac{V_{pv} + R_{sg} I_{pv}}{R_{sgh}} \tag{2}$$

I_{ph} represents the photo current of PV cell which is highly influenced by the temperature according to the Equation (3):

$$I_{ph} = \left(\dfrac{G}{G_{STC}} \right)\left(I_{phn} + K_I \left(T - T_{STC} \right) \right) \tag{3}$$

I_{phn} is the nominal photo current provided at G_{STC}, T_{STC}. The nominal light-generated current can be estimated by Equation (4):

$$I_{phn} = \left(\dfrac{R_s + R_{sh}}{Rs} \right) I_{scn} \tag{4}$$

The diode reverse saturation current I_0 is deduced by the Equation (5):

$$I_0 = \frac{I_{scn} + K_I \Delta T}{e^{\frac{I_{scn} + K_I \Delta T}{aVt}} - 1} \tag{5}$$

where $R_{shg} = N_s \times R_{sh}$ and $R_{sg} = N_s \cdot R_s$.

The PV system consists of a PVG, DC/DC and DC/AC Converters (without energy storage), separated by a DC link voltage, and the main grid. The inductor and capacitor filters store energy, they are represented by square pictograms. Both converters are modeled in average value (Boujmil, Badis, & Nejib Mansouri, 2018).

A capacitor C is needed for controlling the PV output voltage. It is modeled by means of the following equation:

$$R_1 \rightarrow C\frac{du_{pv}}{dt} + \frac{u_{pv}}{R} = i_{pv} - i_L \tag{6}$$

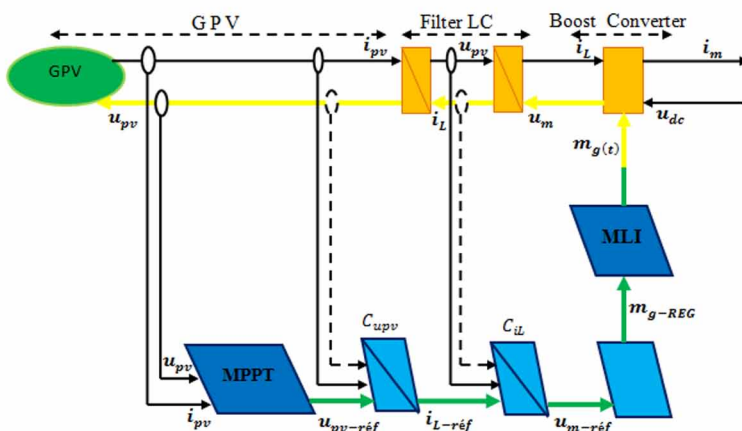An inductor L is used to apply the source alternating rule. It can be modeled by the following differential equation:

$$R_2 \rightarrow L\frac{di_L}{dt} + r.i_L = u_{pv} - u_m \tag{7}$$

$$\begin{cases} R_{m1} \rightarrow u_m = m_g \times u_{dc} \\ R_{m2} \rightarrow i_m = m_g \times i_L \end{cases} \tag{8}$$

m_g is the modulation index.

The EMR of the PVG side is illustrated in Figure 3.

Figure 3. The EMR and its reverse MCS of the PVG side

The dynamics of the DC link and the grid (with the filter) in *dq* reference frame rotating can be expressed by the following relations of the grid side:

$$R_3 \rightarrow C\frac{du_{dc}}{dt} + \frac{u_{dc}}{R} = i_m - i_{mr} \tag{9}$$

$$\begin{cases} R_{m3} \rightarrow \begin{bmatrix} v_{md} \\ v_{mq} \end{bmatrix} = \frac{u_{dc}}{2}\begin{bmatrix} m_d \\ m_q \end{bmatrix} \\ R_{m4} \rightarrow i_{mr} = \frac{1}{2}\left(m_d i_{rd} + m_q i_{rq}\right) \end{cases} \tag{10}$$

$$R_4 \rightarrow \begin{bmatrix} v_{rd} \\ v_{rq} \end{bmatrix} = \begin{bmatrix} P(\theta) \end{bmatrix}\begin{bmatrix} v_{r1} \\ v_{r2} \end{bmatrix} \tag{11}$$

$$R_5 \rightarrow \begin{bmatrix} i_{rd} \\ i_{rq} \end{bmatrix} = \begin{bmatrix} P(\theta) \end{bmatrix}\begin{bmatrix} i_{r1} \\ i_{r2} \end{bmatrix} \tag{12}$$

where:

$$\begin{bmatrix} P(\theta) \end{bmatrix} = \sqrt{\frac{2}{3}}\begin{bmatrix} \cos(\theta) & \cos(\theta - 2\pi/3) \\ -\sin(\theta) & -\sin(\theta - 2\pi/3) \end{bmatrix} \tag{13}$$

$$R_6 \rightarrow (L_1\frac{d}{dt} + r_1)\begin{bmatrix} i_{rd} \\ i_{rq} \end{bmatrix} = \begin{bmatrix} v_{md} \\ v_{mq} \end{bmatrix} - \begin{bmatrix} v_{rd} \\ v_{rq} \end{bmatrix} + \begin{bmatrix} 0 & L_1\omega \\ -L_1\omega & 0 \end{bmatrix}\begin{bmatrix} i_{rd} \\ i_{rq} \end{bmatrix} \tag{14}$$

P and Q powers are computed using the conventional instantaneous power definition in *dq* system, as shown in equation 15:

$$R_7 \rightarrow \begin{bmatrix} p \\ q \end{bmatrix} = \begin{bmatrix} v_{rd} & v_{rq} \\ v_{rq} & -v_{rd} \end{bmatrix}\begin{bmatrix} i_{rd} \\ i_{rq} \end{bmatrix} \tag{15}$$

The objective of this stage is to control the currents injected into the grid. It is needed then to determine the final drives m_{d_reg} and m_{q_reg} to be applied at the entrance of the three-phase inverter according to Equation (16):

$$\begin{cases} m_{d\_reg} = \frac{v_{md\_ref}}{u_{dc}} \\ \\ m_{q\_reg} = \frac{v_{mq\_ref}}{u_{dc}} \end{cases} \tag{16}$$

Thanks to the EMR and MCS, the main system and its control chain consist of first-order nested loops which require a cascade control. This method is characterized by the threefold proprieties:

- Obtaining a cascade system with two or more controllers of any type.
- System stabilization is easier since the subsystems are of the first order.
- Parameter identification of the control system is facilitated. On this topic, the two cascaded loops (inner and outer loop) are tuned simultaneously.

The block diagrams of Figure 4 and Figure 5 are obtained.

PRESENTATION OF THE DIFFERENT CONTROL STRATEGIES

Choosing an accurate and simple control strategy is crucial since it ensures high performances and low costs of the grid connected PV system. The control chain consists of two main parts including the PVG side control which ensures the maximum power extraction from the PVG by using the appropriate MPPT (P&O), and the grid side control by controlling the DC link voltage and injecting the desired power to the grid. In this context, metaheuristic algorithms have become nowadays powerful tools for the purpose of solving complex optimization issues. Compared to several methods based on challenging mathematical programming, these metaheuristic algorithms are generally more reliable to obtain meaningful parameters and is simple and easy to implement.

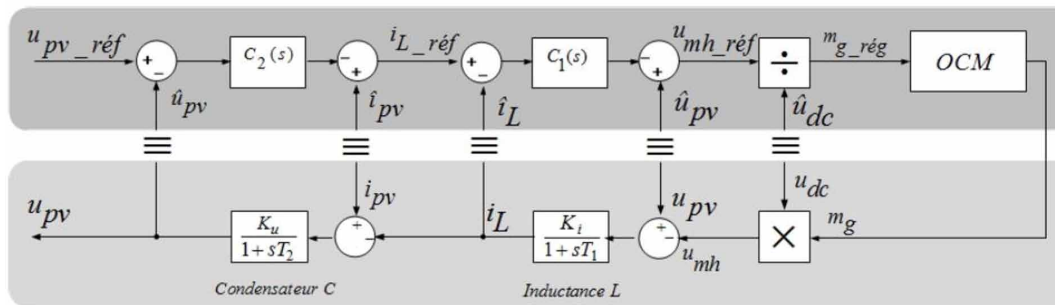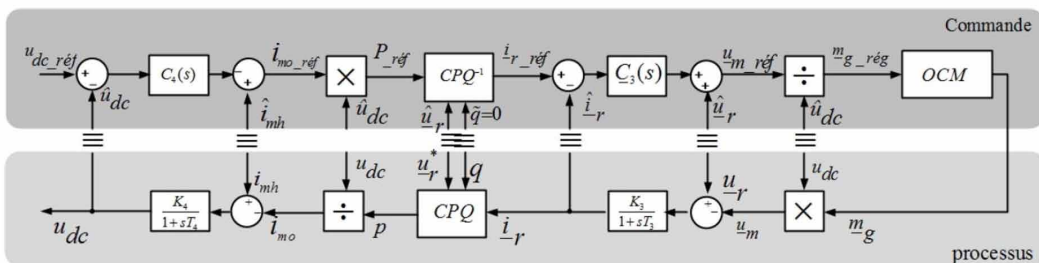**Figure 4. Block diagram of the PVG side**

Figure 5. Block diagram of the grid side

PSO-PID

The PSO is a population-based evolutionary algorithm used for solving the complex optimization problems iteratively (Badis, Boujmil, & Mansouri, 2017). PSO imitates the behavior of birds and each individual of the birds swarm represents candidate solution that moves in the multi-dimensional search space in order to find the best solution. This stochastic algorithm is applied in order to optimize the gains of the controllers to ensure the optimal control performance. First, a population of PID gains (K_P, K_I, K_D) is randomly assessed and set into movement. Moves are made according to a simple relation exploiting the position and velocity of each particle.

Each particle represents a candidate solution for the PID parameters. The position of each candidate is adjusted according to the local best position (P_{best}) through the current particles and the global best (G_{best}) position through the entire population according to the following equation:

$$x_i^{k+1} = x_i^k + \Phi_i^{k+1} \tag{17}$$

where the velocity component Φ_i which represents the velocity step is calculated as follows:

$$\Phi_i^{k+1} = \omega \Phi_i^k + c_1 r_1 \left\{ P_{best} - x_i^k \right\} + c_2 r_2 \left\{ G_{best} - x_i^k \right\} \tag{18}$$

Finally, when a specified stopping criterion is met or a maximum number of iteration is reached, the algorithm is ended. The swarm size is the number of particles in a population. It is set to 20 in this study. A suitable set of PID controller parameters gives a good system response and leads to a minimized performance index under consideration. The specific values of the PSO algorithm parameters are given by Table 1.

ACO-PID

ACO is population-based metaheuristic which is originally introduced in 2005 and used further for solving complex combinatorial problems. ACO is inspired by the foraging behavior of ants, in other words, how to find the shortest path. First, a pheromone model T, which represents a probability distribution all over the search space, is defined (Dhieb, Yaich, Guermazi, & Ghariani, 2019). Ants move (initially) randomly, and when they find food, they return to their colony leaving pheromone trails. If other ants find such a path, they are likely not to continue moving randomly, but rather follow the same path. Ants are driven by a probability rule to choose their solution to the problem. Equation (19) describes the probability that the ant will move between the two nodes i and j:

$$p_{ij} = \frac{\left[\tau_{ij} \right]^\alpha \left[\eta_{ij} \right]^\beta}{\sum\limits_{j \in noeuds} \left[\tau_{ij} \right]^\alpha \left[\eta_{ij} \right]^\beta} \tag{19}$$

Table 1. Properties of the PSO algorithm

Population size of swarm	20
Inertia weight ω	0.9
Social parameter C_1	2
Cognitive parameter C_2	2

At each iteration, the pheromone value is modified and research becomes concentrated in regions with high-quality solutions (Dorigo, & Blum, 2005).

η_{ij} is the inverse of the distance between the two nodes i and j.

The parameters are related to the ACO algorithm.

As the ants move between nodes, the pheromone level function on the selected edge is updated according to equation (20):

$$\tau_{ij} = \left(1 - \rho\right)\tau_{ij} + \rho\tau_{0} \tag{20}$$

with $\rho \in \left[0, 1\right]$.

τ_{0} is the initial value of the pheromone deposited on each of the edges (i, j). The specific values of the ACO algorithm parameters are given by Table 2.

GA Based Control Strategy

Genetic Algorithms: Basic Concepts

GA is a population-based metaheuristic optimization algorithm. It is a direct, stochastic, parallel method which is originally introduced by Holland (Holland, 1962). It mimics the biological evolution of the living beings and relies on three fundamental operators on every generation namely the selection, crossover, and mutation. The fundamental idea of GA consists on operating on a finite population of N chromosomes (Badis, Boujmil, & Mansouri, 2017). The survival of the fittest principle is applied so that the overall quality of solutions is improved as the algorithm evolves from one generation to the next (Tarik, Zerhouni, Stambouli, Tioursi, & M'harer, 2017). The evolutionary cycle can be summarized by the flowchart in Figure 6.

Fractional-Order PID Controller

The generalized open-loop transfer function of the FOPID controller used in this research is given by equation (21) (Badis, Mansouri, & Boujmil, 2019):

$$C(s) = \frac{U(s)}{E(s)} = K_P + \frac{K_I}{s^\lambda} + K_D s^\mu, \left(\lambda, \mu \geq 0\right) \tag{21}$$

where C(s) indicates the controller output, U(s) is the control signal and E(s) represents the error signal. K_P, K_I, K_D are the proportional, integral and derivative parameters, respectively. λ is the order of integration, and μ is the order of differentiation. Typically, researchers use either a range of 0 to 2 as the order of λ and μ of the FOPID.

Table 2. Properties of the ACO algorithm

Ant number	20
α	0.8
β	0.2
γ, ρ	0.7

Figure 6. Genetic Algorithm based tuning flowchart
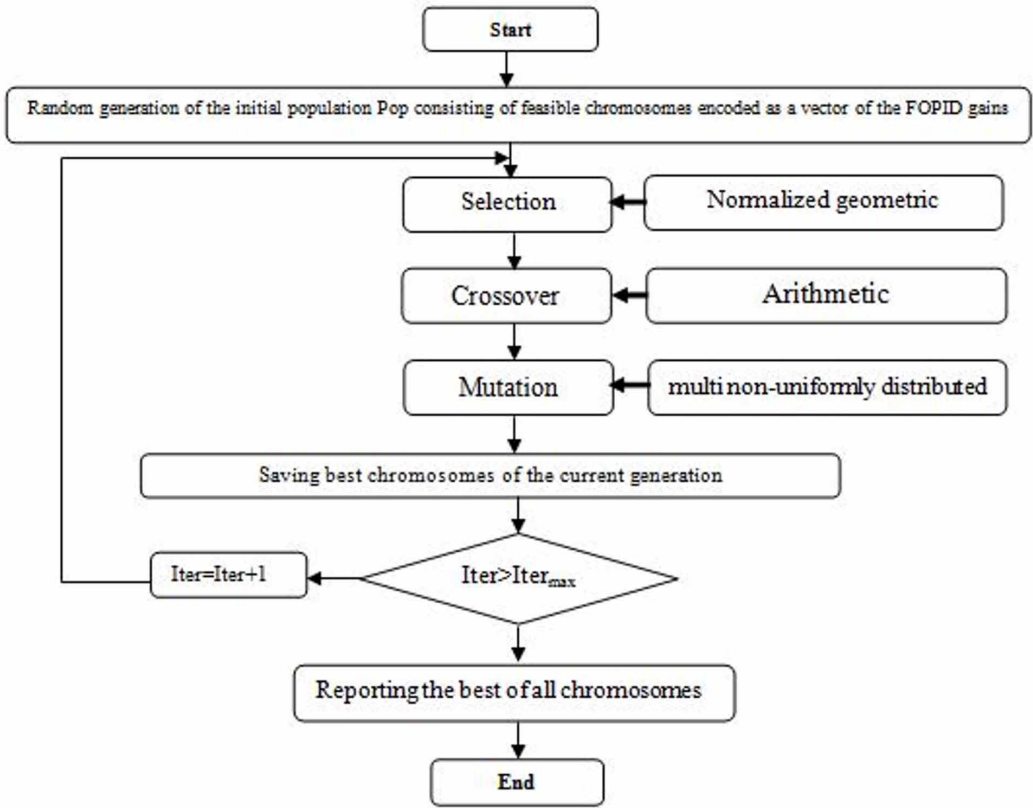
GA Based FOPID Controller Tuning

The GA-FOPID proposed strategy is designed to tune the parameters of the FOPID controller and to maintain the stability of the whole control system.

First, FOPID gains are randomly generated individuals in the first population forming a mating pool. Then, they are used to control each subsystem of the grid-connected PV system. The selection operator is applied to it to choose the parent with higher fitness for insertion in the next generation. Once this process is completed, the crossover operator is initiated. It is based on the capture of the best parts of parent chromosomes in order to create better new offspring. A crossover probability P_{cross} which indicates how often the operator, is fixed.

Finally, the introduction of mutation is the solution for the diversity lack, which makes the GA searches the whole problem space (Badis, Mansouri, & Sakly, 2016).

In every control loop, the chromosome which consists of a set of FOPID gains is passed to the global system so as to compute its complete response. At each iteration, each chromosome has to be evaluated via the Fitness function which is imperative to evaluate the best FOPID controller parameters for each loop in the system. In fact, the Fitness function is created in order to search for the FOPID parameters that convey the fastest rise time and the smallest overshoot. Over time, the quality of the solution is expected to improve.

The GA parameters used to generate the initial random population of candidates representing the PID parameters (K_P, K_I, K_D) and the FOPID parameters (K_P, K_I, K_D, λ, μ) are listed in Table 3.

Table 3. GA-Parameters of the controllers

Population size	30
Variable Bounds	$[K_P; K_I; K_D; \lambda; \mu] = [0\ 500;\ 0\ 500;\ 0\ 500;\ 0\ 2;\ 0\ 2]$
Crossover rate	0.9
Mutation rate	0.01

The choice of a small population size is made in order to allow the FOPID controller to be raised as fast as possible. Besides, the inner loops must reach the steady state faster than the outer loop to avoid oscillations in both two loops.

Fitness Function

The ITAE criterion reduces the response time that cannot be achieved with IAE or ISE. The ITAE criterion also reduces overshoot. It has been reported that ITAE is a better objective function in several studies. Therefore, in this paper, ITAE is used as an objective function to optimize the gains of the FOPID/FOPID controller.

In order to tune the controller with the appropriate algorithms, an optimization problem is first formulated which requires the generation of a Fitness Function. For each loop in the system, the performance of the controller is evaluated according to the Fitness Function described in Equation (22) and (23):

$$overshoot = \max\left(Y_{out}\right) - Y_{ref} \tag{22}$$

$$F = \alpha.overshoot + \beta.ITAE \tag{23}$$

As there is no preference between the two objectives, $\alpha = \beta = 0.5$.

MPPT (P&O) Control

The objective of the MPPT is to extract the MPP from the solar array. Recently, many MPPT techniques have been developed and improved continuously. The P&O method is widely applied due to its simplicity and ease of implementation. The MPPT algorithm repeats itself periodically using the Power P and the previous Power P_{old} until the optimal operating point is reached. The system then oscillates near the MPP. The algorithm then seeks to impose a reference voltage to maximize power. Since it is easy to use and implement and is not the main focus of our study, P&O was therefore used as the basis for this work (Badis, Mansouri, & Sakly, 2016).

SIMULATION RESULTS AND DISCUSSION

For the purpose of testing the effectiveness of the proposed control strategies under different operating conditions, the instantaneous average model of the entire system is developed. Simulation results are carried out under the same conditions:

P=1kw, C=220μf, R=100K, L=23mH, C_1=5000μf, R_1=10K, r_1=0.0002, L_1=1mH, U_r=380v, f=50Hz

Control Under Sudden Irradiation Variations

For the case of sudden irradiation change, the irradiation moves from one level to a higher one, and then returns to a lower level again in order to evaluate the performance of the proposed techniques as depicted in Figure 7.

In case of constant temperature, when irradiation variation occurs, the feasibility of MPP tracking is demonstrated for the P&O method. Therefore, the power injected into the grid is optimized since the maximum PV current and voltage are extracted. Figure 8 shows the results obtained with the P&O method. These results illustrate the good tracking in case of abrupt changes in irradiation.

Stage 1: PVG Side Control

The process and its control chain of the PVG side are represented in Figure 9. The control of the PVG is made up of two cascaded loops. This structure requires two controllers $C_1(s)$ and $C_2(s)$ which respectively affect the current i_L and the voltage U_{pv}.

The PVG side cascade control needs two controllers for the outer loop (U_{pv} voltage loop) and the inner loop (the I_L current loop). The response time of the inner loop has to be configured to be

Figure 7. Illumination variation
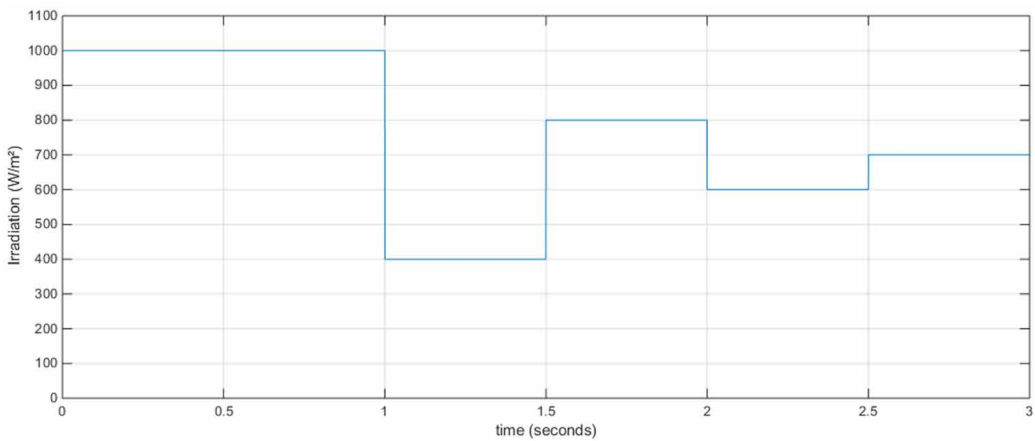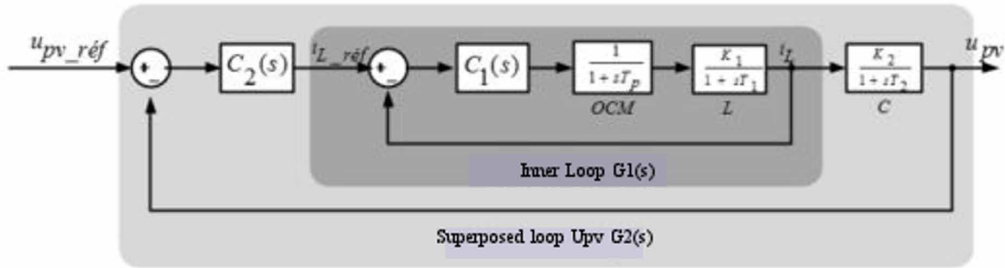

Figure 8. P-V curve with P&O
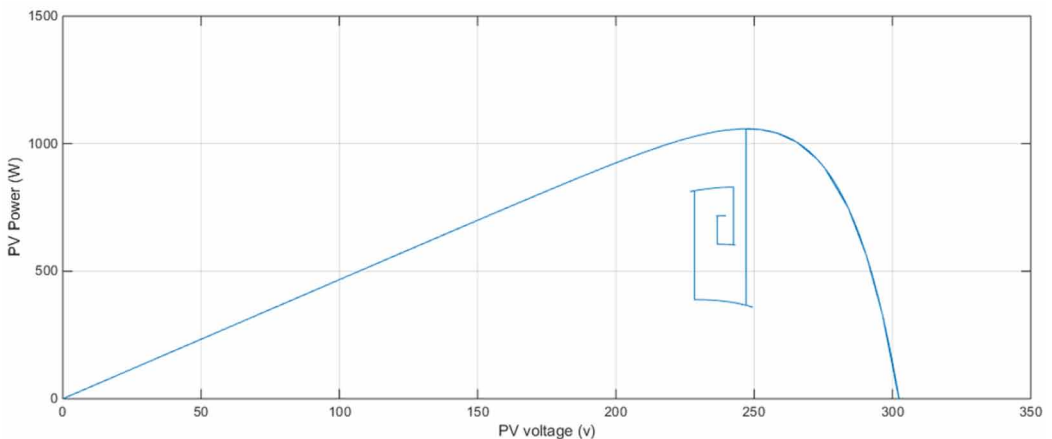
Figure 9. The simplified block diagram of the process

shorter than the outer loop response time in order to correct the error rapidly. The performance of all the metaheuristic algorithms is tested. The parameter optimization of the cascaded system is carried out simultaneously. The algorithm gradually minimizes the Fitness Function and saves the optimized gains giving the best performance. The algorithm ends if the value of the fitness function is kept constant over a few successive iterations.

The gains of the controllers on the PVG side are summarized in Table 4 for each method. Tuning the PVG side controllers is obtained simultaneously since the output of the inner process feeds the external loop. Giving better performance, PI and FOPI controllers can be employed to replace the PID and FOPID controllers, due to the small order of the subsystems.

The simulation results are displayed in Figure 10 for the PVG control. From the results, it can be seen that the GA-FOPID controller performs the best in terms of reference tracking, while the ACO-PID is not as reliable as the PSO-PID and the GA-PID. When irradiance is changed from one

Table 4. Control Gains

		Controller parameters	K_p	K_i	K_d	Λ	μ
PVG side control	Current loop I_L	PSO-PID	166.7585	617.1194	0	_	_
		GA-PID	199.4052	248.3750	9.9269	_	_
		ACO-PID	0.67797	0.89969	0.18383	_	_
		GA-FOPID	16.34	0.4127	2.814	0.00042	0
	Voltage loop U_{pv}	PSO-PID	0.3448	0.0869	0	_	_
		GA-PID	0.2797	0.0983	0	_	_
		ACO-PID	0.6232	2.3787	0	_	_
		GA-FOPID	22.41	0.145	0	0.1033	0
Grid side control	DC link voltage loop U_{dc}	PSO-PID	10	10	0	_	_
		GA-PID	1.1270	0.0871	0	_	_
		ACO-PID	0.4633	0.5796	0	_	_
		GA-FOPID	0.50140	0.0068	0	1.0748	0.08004
	Grid current loop i_{dq}	PSO-PID	1564459.7903	2.3633	0	_	_
		GA-PID	0.2797	0.0983	0	_	_
		ACO-PID	0.0803	1.07	0.3727	_	_
		GA-FOPID	0.2783	0.0095	0	1.1049	0.3005

Figure 10. U$_{pv}$ voltage at varying irradiation
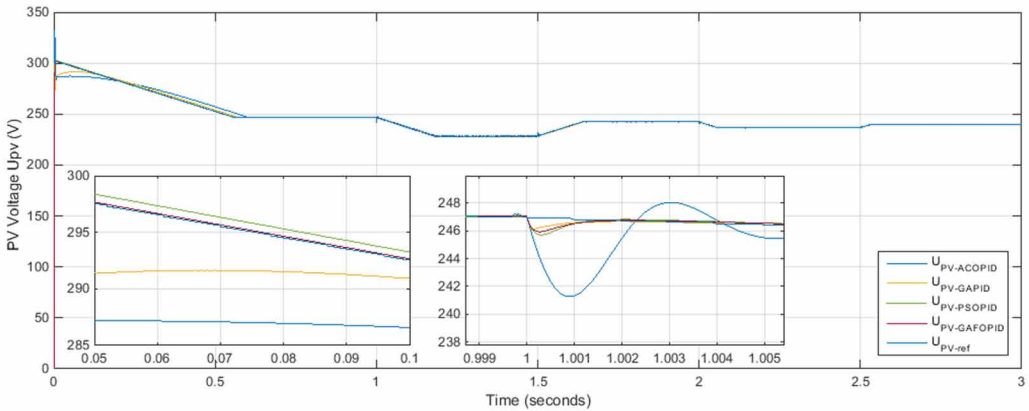
level to another, GA-FOPID, PSO-PID and GA-PID follow the new power level quickly. However, the ACO-PID requires more time to find the steady state (Trise=0.5s).

Stage 3: Grid Side Control

The main purpose of the grid side control is to maintain the DC bus voltage U$_{dc}$ constant regardless the input variation.

Figure 12 shows that the proposed control techniques portray good performances through the perfect follow-up of the DC link voltage in spite of the irradiation variation. In fact, the U$_{dc}$ is maintained at the same value (700V) and promptly reduces the error if sudden change occurs.

Table 4 enumerates the controller gains of the grid current loop (inner loop) and the controller gains of the DC link voltage loop (superposed loop) as depicted in Figure 11.

Under this condition, the performance of the designed controllers is verified when solar irradiation varies. The MPPT will follow the maximum power although there are variations in the atmospheric conditions. Therefore, the amount of energy supplied to the grid will be changed since the output current of the PVG will change as shown in Figure 13, Figure 14, Figure 15 and Figure 16. It can be seen that the grid current varies considerably with the irradiation variation.

Figure 11. Block diagram of the inner loop on the grid side in the Park frame
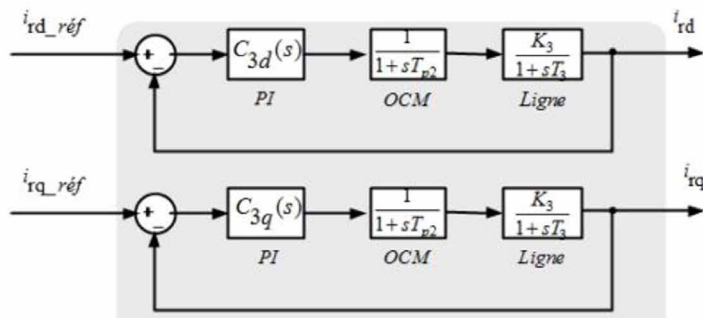
Figure 12. U$_{dc}$ link voltage at varying irradiation
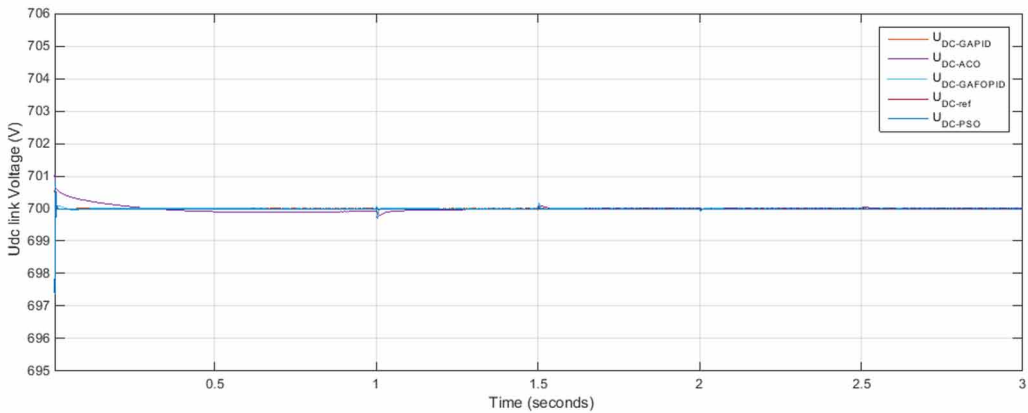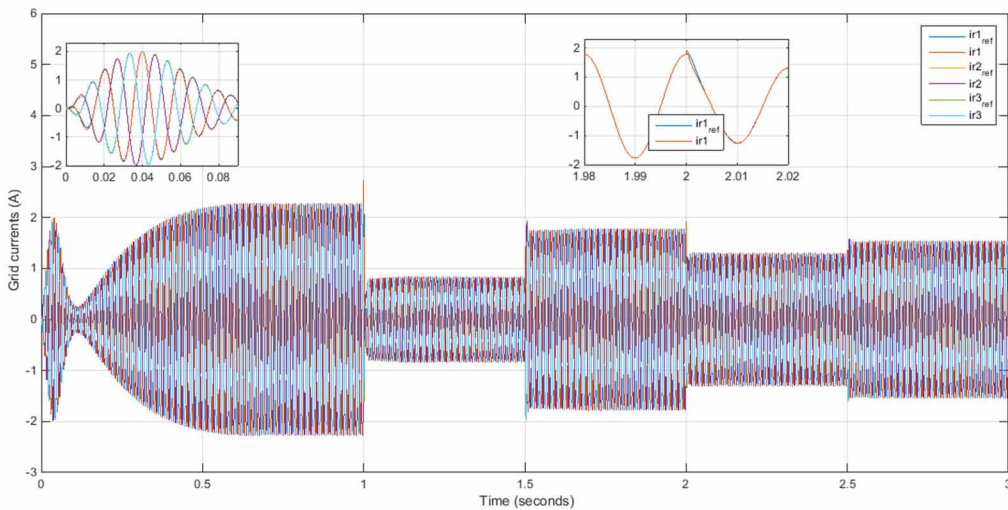

Figure 13. Grid Currents (GA-FOPID Control)

GA-FOPID controller is effective in the transient and the steady state as well as compared to the other techniques.

Control Under Voltage Dips Without Current Limitation

The main objective of the proposed control strategies is to keep the DC link voltage constant regardless of the power variation. With a constant irradiance G=1000G/m², Figures 18 and 19 highlight the impact of a grid voltage dip as shown in Figure 17 on the grid currents and DC link voltage.

Results prove that all techniques performed approximately the same. Indeed, Figure 19 validates that the DC link voltage controller forces the measured U$_{dc}$ to follow its reference when the system experiences a voltage dip at t=[0.8s, 0.9s] without limiting the amplitude of the grid current. As shown in Figure 18, this default implies an increase in grid currents, while U$_{dc}$ is maintained at the same value due to the P&O algorithm.
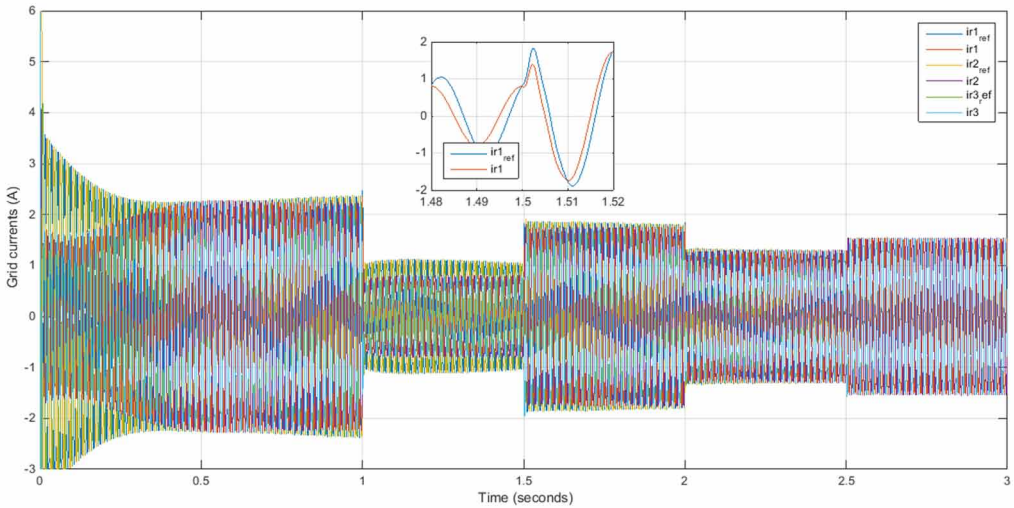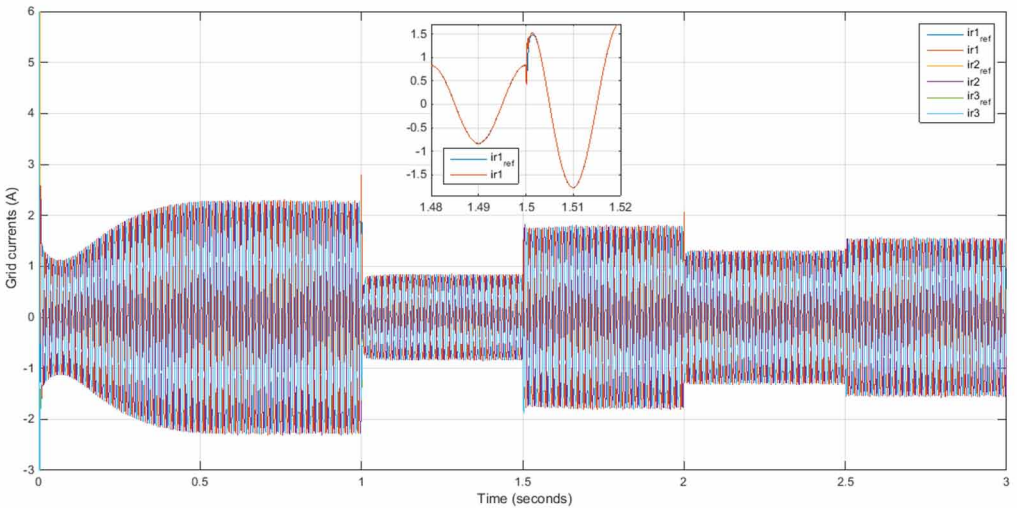
Figure 14. Grid currents (ACO-PID Control)

Figure 15. Grid Currents (GA-PID)

Control Under Voltage Dips With Current Limitation

Figure 20 and Figure 21 also show how the same grid voltage dip affects the DC link voltage and the grid currents with a limitation of their amplitudes. Such a limitation causes an increase of the DC link voltage. If such a defect occurs, the control techniques are proven to be robust.

Control Under Parametric Variation

A step-down of 50% of the resistance r_1 at t=0.8s results in an increase in the time constant (T1=L1/r1) by 100%. Simulation results provided in Figure 22 show the efficiency of the proposed GA-based control when experiencing sudden parametric variations over other controllers. GA-FOPID based control can inject the desired output power into the grid with unity power factor. On the other hand,
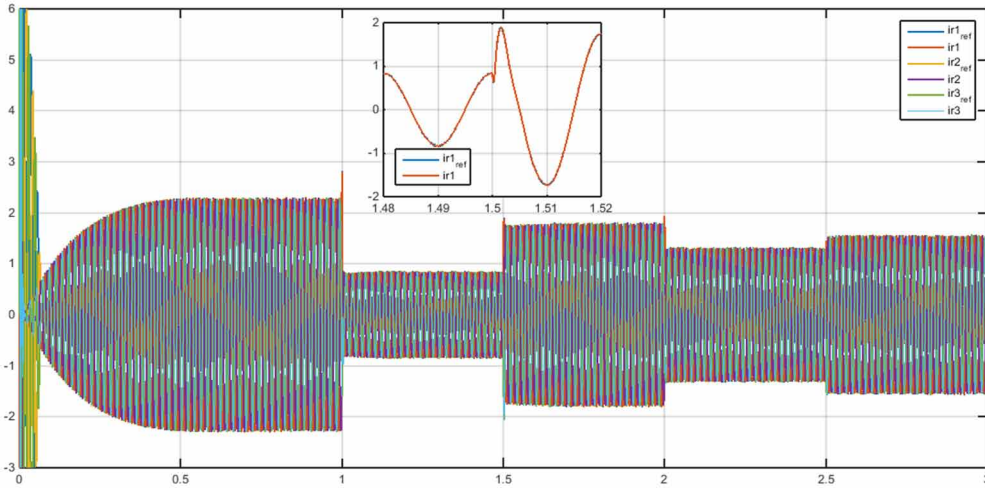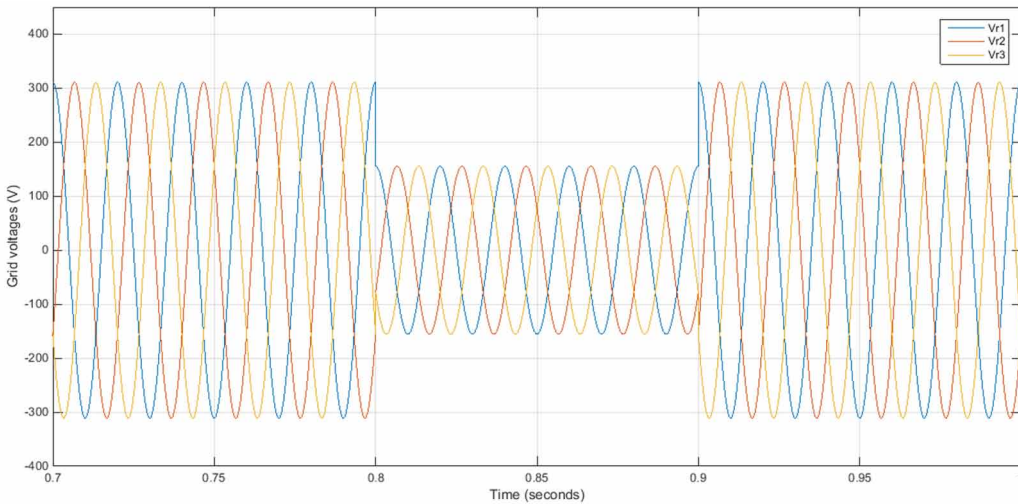
Figure 16. Grid Currents (PSO-PID)

Figure 17. Voltage dip at t=[0.8s, 0.9s]

ACO-PID based control is unable to overcome this issue as the steady state has not been reached yet when the resistance value variation occurs.

Table 4 gives a summary of controllers gains used for the results obtained above for the PVG side control (Current loop I_L and Voltage loop U_{pv}) and the grid side (DC link voltage loop U_{dc} and Grid current). This table shows that in the case of the use of the intelligent controller, the GA-FOPID gives the best results and brings a clear improvement to the power factor compared to the other control techniques thanks to the use of five parameters (K_P, K_I, K_D, λ, μ).

The GA-FOPID algorithm has to gradually and iteratively minimize the performance index (Fitness Function) in order to find the optimal parameters for the FOPID/FOPID cascade controllers of the inner and outer loop. For instance, when the algorithm completes, the value of the fitness

Figure 18. Voltage dip effect on grid currents without limitation by using: A: PSO-PID; B: GA-PID; C: ACO-PID; D: GA-FOPID
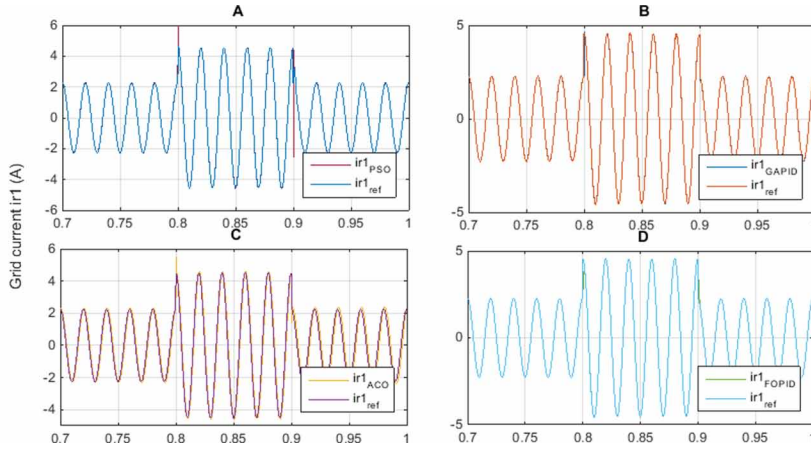

Figure 19. Voltage dip effect on DC link voltage without limitation by using: A: PSO-PID; B: GA-PID; C: ACO-PID; D: GA-FOPID
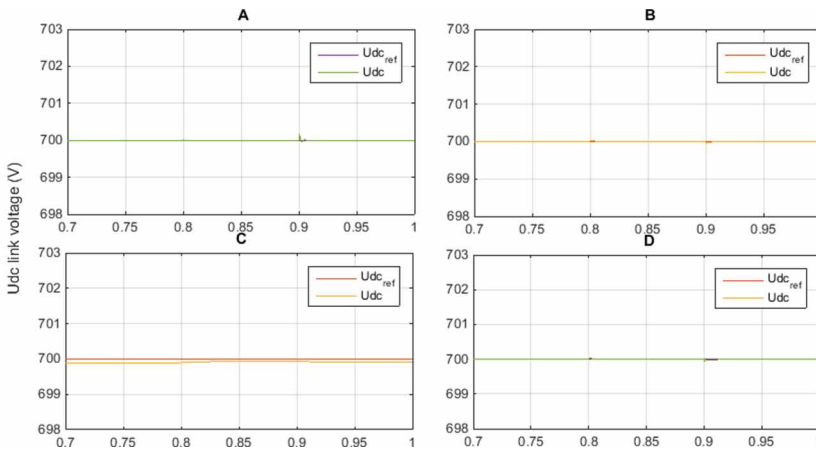

Figure 20. Voltage dip effect on grid currents with limitation by using: A: PSO-PID; B: GA-PID; C: ACO-PID; D: GA-FOPID
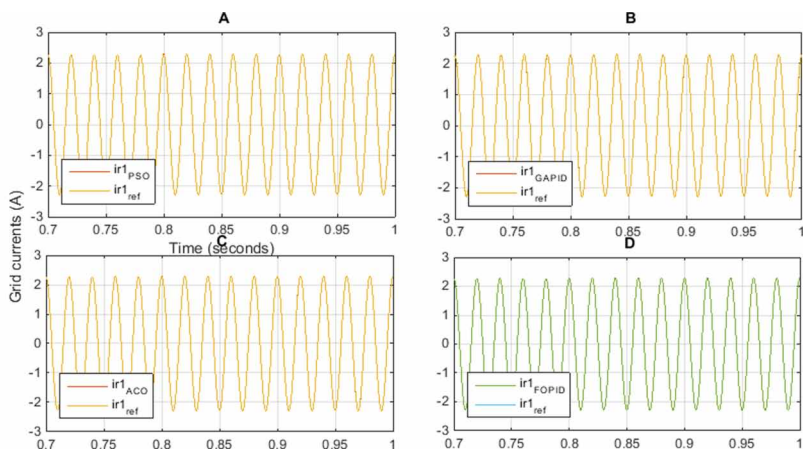
Figure 21. Voltage dip effect on DC link voltage with limitation by using: A: PSO-PID; B: GA-PID; C: ACO-PID; D: GA-FOPID
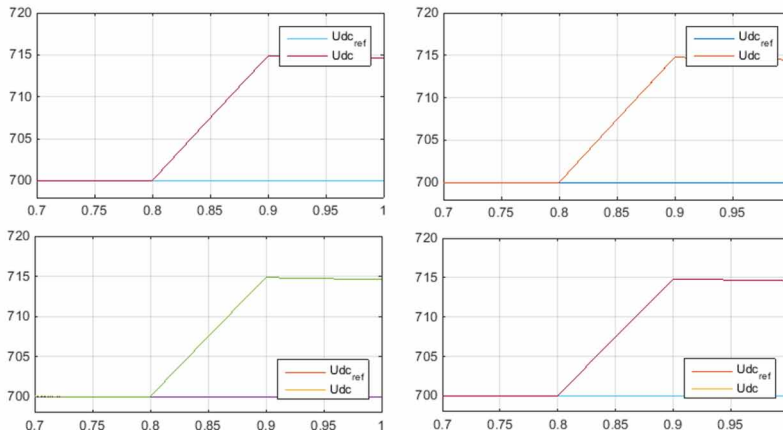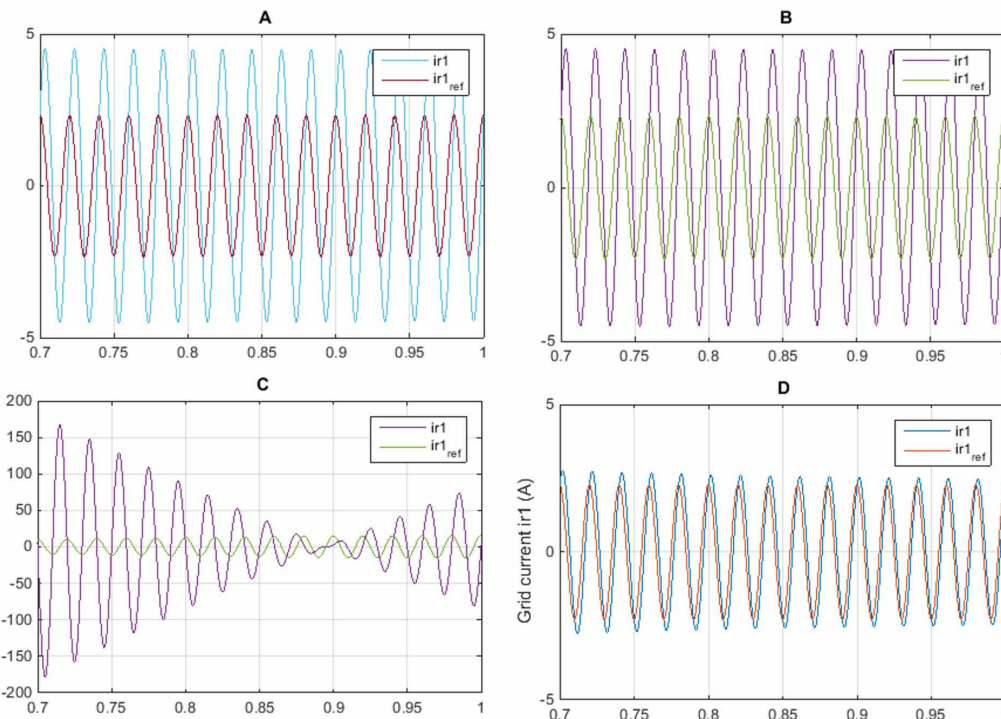

Figure 22. The effect of line resistance sudden decrease on the grid currents by using: A: PSO-PID; B: GA-PID; C: ACO-PID; D: GA-FOPID

function is kept constant over a few successive iterations as shown in Figure 23 and Figure 24 for the inner and outer loop respectively on the GPV side.

Simulations are carried out with a small population size. This specification is crucial in order to guarantee a faster tuning. In this research, the initial population size as well as the maximum number of iterations are set to 30 for all control loops.

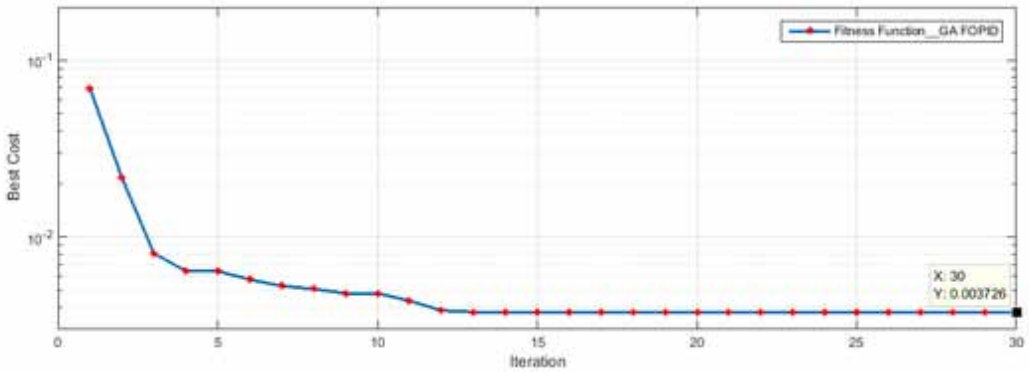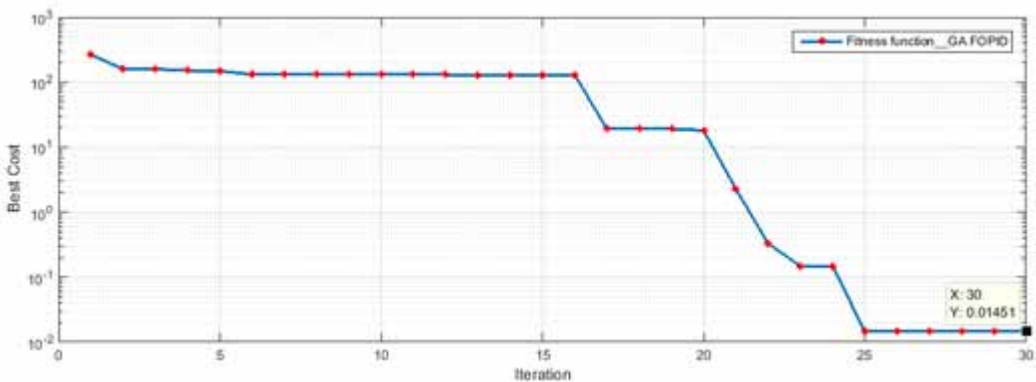**Figure 23. Convergence of the fitness function of the inner loop i$_L$**

Figure 24. Convergence of the fitness function of the outer loop U$_{pv}$

The best population can be graphically represented as an insight on how the GA-FOPID algorithm converges to the optimal parameters of the inner loop, as shown in Figure 25 and the outer loop as represented in Figure 26 of the PVG control side. Giving better performance, FOPI controllers can be used instead of FOPID controllers, thanks to the reduced order of the inner loop subsystems.

CONCLUSION

A novel cascade control technique based on GA-FOPID is proposed for controlling cascade loops in a grid connected PV system. This technique generates randomly a number of solutions in order to converge towards the global solution. The algorithm searches simultaneously for the five parameters of each controller that most optimize the power transfer from the PVG to the grid. A comparative assessment of three controllers is presented in this paper, namely GA-FOPID, GA-PID, PSO-PID, and ACO-PID for a grid connected PV system. Performances of the controllers are compared when fast-changing solar irradiation, voltage dip and parametric variations of the system are experienced. Simulations are executed by means of Matlab/Simulink to conclude that GA based FOPID control defeats other techniques.

Figure 25. Convergence of the GA-FOPID algorithm through the iterations of U$_{pv}$
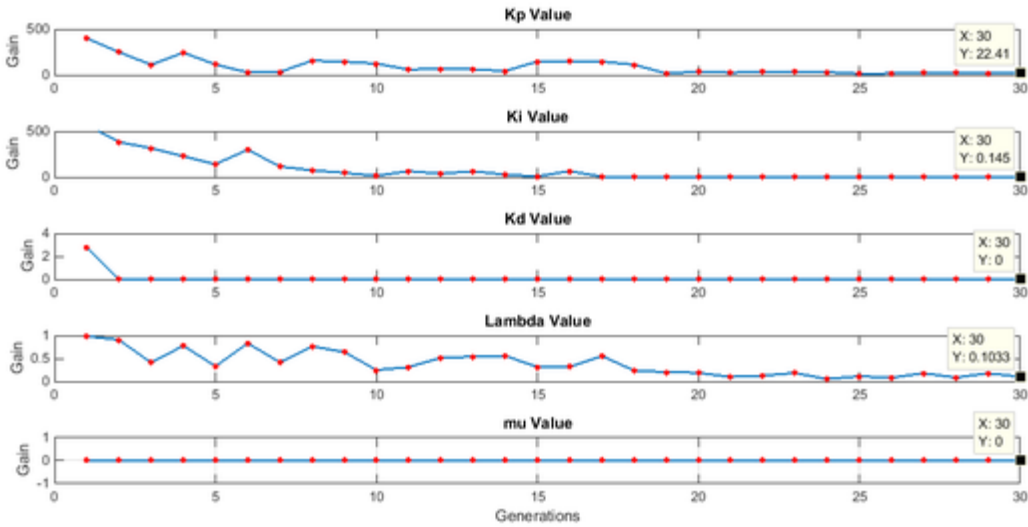

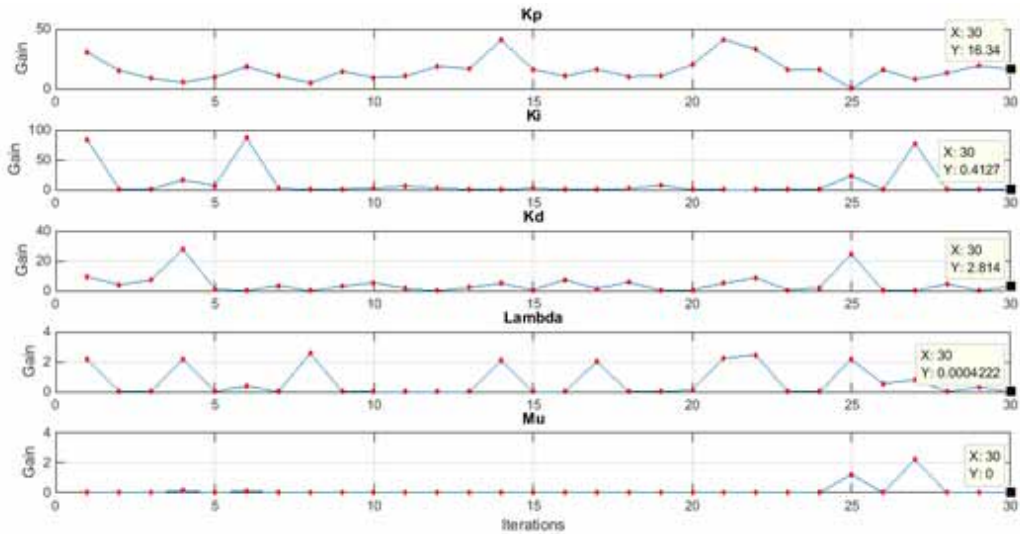
Figure 26. Convergence of the GA-FOPID algorithm through the iterations of I$_L$

Moreover, for superior tracking efficiency, a P&O based MPPT algorithm is employed to extract maximum power from PV panels.

The authors are intending to improve the designed control technique in order to have better performances under any circumstances, especially when the PVG suffers from Partial Shading.

REFERENCES

Alajmi, B. N., Ahmed, K. H., Finney, S. J., & Williams, B. W. (2011). Fuzzy-logic-control approach of a modified hill-climbing method for maximum power point in microgrid standalone photovoltaic system. *IEEE Transactions on Power Electronics*, *26*(4), 1022–1030. doi:10.1109/TPEL.2010.2090903

Badis, A., Boujmil, M. H., & Mansouri, M. N. (2017). A Comparative Study on Maximum Power Point Tracking Techniques of Photovoltaic Systems. *International Journal of Energy Optimization and Engineering*, *7*(1), 66–85. doi:10.4018/IJEOE.2018010104

Badis, A., Mansouri, M. N., & Boujmil, M. H. (2019). Cascade control of grid-connected PV systems using TLBO-based fractional-order PID. *International Journal of Photoenergy*, *2019*, 1–17. Advance online publication. doi:10.1155/2019/4325648

Badis, A., Mansouri, M. N., & Sakly, A. (2016, March). PSO and GA-based maximum power point tracking for partially shaded photovoltaic systems. In *Renewable Energy Congress (IREC), 2016 7th International* (pp. 1-6). IEEE. doi:10.1109/IREC.2016.7478923

Boujmil, M. H., Badis, A., & Nejib Mansouri, M. (2018). Nonlinear Robust Backstepping Control for Three-Phase Grid-Connected PV Systems. *Mathematical Problems in Engineering*, *2018*, 1–13. Advance online publication. doi:10.1155/2018/3824628

Boumaaraf, H., Talha, A., & Bouhali, O. (2015). A three-phase NPC grid-connected inverter for photovoltaic applications using neural network MPPT. *Renewable & Sustainable Energy Reviews*, *49*, 1171–1179. Advance online publication. doi:10.1016/j.rser.2015.04.066

Chen, Y., Bhaskaran, T., & Xue, D. (2008). Practical Tuning Rule Development for Fractional Order Proportional and Integral Controllers. *Journal of Computational and Nonlinear Dynamics*, *3*(2), 021403. doi:10.1115/1.2833934

Das, S., Pan, I., Das, S., & Gupta, A. (2012). Improved model reduction and tuning of fractional-order PIλDμ controllers for analytical rule extraction with genetic programming. *ISA Transactions*, *51*(2), 237–261. doi:10.1016/j.isatra.2011.10.004 PMID:22036301

Dhieb, Y., Yaich, M., Guermazi, A., & Ghariani, M. (2019). PID controller tuning using ant colony optimization for induction motor. *Journal of Electrical Systems*, *15*(1), 133–141.

Dorigo, M., & Blum, C. (2005). Ant colony optimization theory: A survey. *Theoretical Computer Science*, *344*(2-3), 243–278. doi:10.1016/j.tcs.2005.05.020

Ganesan, T., Vasant, P., Sanghvi, P., Thomas, J., & Litvinchev, I. (2020). Random Matrix Generators for Optimizing a Fuzzy Biofuel Supply Chain System. *Journal of Advanced Engineering and Computation*, *4*(1), 33. doi:10.25073/jaec.202041.268

Green, M. A. (2002). Photovoltaic principles. In *Physica E* (Vol. 14, pp. 11–17). Low-Dimensional Systems and Nanostructures. doi:10.1016/S1386-9477(02)00354-5

Holland, J. H. (1962). Outline for a logical theory of adaptive systems. *Journal of the Association for Computing Machinery*, *9*(3), 297–314. doi:10.1145/321127.321128

Hu, J., Zhu, J., & Dorrell, D. G. (2015). Model predictive control of grid-connected inverters for PV systems with flexible power regulation and switching frequency reduction. *IEEE Transactions on Industry Applications*, *51*(1), 587–594. doi:10.1109/TIA.2014.2328785

Jeba, P., & Immanuel Selvakumar, A. (2018). FOPID based MPPT for photovoltaic system. *Energy Sources. Part A, Recovery, Utilization, and Environmental Effects*, *40*(13), 1591–1603. doi:10.1080/15567036.2018.1486480

Kaya, I., Tan, N., & Atherton, D. P. (2007). Improved cascade control structure for enhanced performance. *Journal of Process Control*, *17*(1), 3–16. doi:10.1016/j.jprocont.2006.08.008

Kennedy, J., & Eberhart, R. (1995). Particle swarm optimization. In *Proceedings of ICNN'95-international conference on neural networks* (Vol. 4, pp. 1942-1948). IEEE. doi:10.1109/ICNN.1995.488968

Koad, R. B. A., Zobaa, A. F., & El-Shahat, A. (2017). A Novel MPPT Algorithm Based on Particle Swarm Optimization for Photovoltaic Systems. *IEEE Transactions on Sustainable Energy*, *8*(2), 468–476. doi:10.1109/TSTE.2016.2606421

Koutroulis, E., & Blaabjerg, F. (2015). Overview of Maximum Power Point Tracking Techniques for Photovoltaic Energy Production Systems. *Electric Power Components and Systems*, *43*(12), 1329–1351. doi:10.1080/15325008.2015.1030517

Lhomme, W., Delarue, P., Giraud, F., Lemaire-Semail, B., & Bouscayrol, A. (2012, September). Simulation of a photovoltaic conversion system using energetic macroscopic representation. In *Power Electronics and Motion Control Conference (EPE/PEMC), 2012 15th International*. IEEE. doi:10.1109/EPEPEMC.2012.6397361

Liu, T., Gu, D., & Zhang, W. (2005). Decoupling two-degree-of-freedom control strategy for cascade control systems. *Journal of Process Control*, *15*(2), 159–167. doi:10.1016/j.jprocont.2004.06.001

Malaterre, P. O., Dorchies, D., & Baume, J. P. (2014). Automatic tuning of robust PI controllers for a cascade of rivers or irrigation canals pools. In *2014 European Control Conference, ECC 2014* (pp. 2780–2785). doi:10.1109/ECC.2014.6862508

Menniti, D., Pinnarelli, A., & Brusco, G. (2011). *Implementation of a novel fuzzy-logic based MPPT for grid-connected photovoltaic generation system. In 2011 IEEE PES Trondheim PowerTech: The Power of Technology for a Sustainable Society*. POWERTECH. doi:10.1109/PTC.2011.6019369

Petráš, I., Dorčák, Ľ., & Koštial, I. (1998). Control quality enhancement by fractional order controllers. *Acta Montanistica Slovaca Ročník*, *3*(2), 143–148. https://actamont.tuke.sk/pdf/1998/n2/10petras.pdf

Raducu, G. A. (2008). *Control of grid side inverter in a B2B configuration for WT applications*. Aalborg University.

Singh, D., & Padhy, P. K. (2017). *Design and tuning of PIλDμ controller for higher order process using PSO-NM. In 2017 Innovations in Power and Advanced Computing Technologies, i-PACT 2017*. doi:10.1109/IPACT.2017.8245218

Solihin, M. I., Tack, L. F., & Kean, M. L. (2011). Tuning of PID Controller Using Particle Swarm Optimization (PSO). *International Journal on Advanced Science, Engineering and Information Technology*, *1*(4), 458. doi:10.18517/ijaseit.1.4.93

Tarik, B. M., Zerhouni, F. Z., Stambouli, A. B., Tioursi, M., & M'harer, A. (2017). Parameter Optimization of Photovoltaic Solar Cell and Panel Using Genetic Algorithms Strategy. In Nature-Inspired Computing: Concepts, Methodologies, Tools, and Applications (pp. 1371-1390). IGI Global. doi:10.4018/978-1-5225-0788-8.ch052

Tayal, K., & Ravi, V. (2016). Particle swarm optimization trained class association rule mining: Application to phishing detection. In *ACM International Conference Proceeding Series*. doi:10.1145/2980258.2980291

Thumu, R., & Harinadha Reddy, K. (2019). PI, fuzzy based controllers for FACTS device in Grid Connected PV system. *International Journal of Integrated Engineering*, *11*(6), 176–185. doi:10.30880/ijie.2019.11.06.019

Tyukhov, I., Rezk, H., & Vasant, P. (2016). Modern Optimization Algorithms and Applications in Solar Photovoltaic Engineering. *Sustaining Power Resources through Energy. Optimization and Engineering*, 390–445.

Xu, G., Moulema, P., Ge, L., Song, H., & Yu, W. (2016). A Unified Framework for Secured Energy Resource Management in Smart Grid. *Smart Grid*, 73–96.

Yang, B., Li, W., Zhao, Y., & He, X. (2010). Design and Analysis of a Grid-Connected Photovoltaic Power System. *IEEE Transactions on Power Electronics*, *25*(4), 992–1000. doi:10.1109/TPEL.2009.2036432

Afef Badis was born in Tunisia, in 1989. She received the Electrical Engineering diploma in 2013 from the National Engineering school of Monastir (ENIM). She is currently working toward the PhD in the control of photovoltaic energy injected into the three-phase grid. Her research interests are modeling, simulation, and the design of electronic power systems, in particular, the grid-connected PV systems.